Occupancy-based Buildings-to-grid Integration Framework for Smart and Connected Communities

Abstract

Buildings-to-grid (BtG) integration simulations are becoming prevalent due to the development of smart buildings and smart grid. Buildings are the major energy consumers of the total electricity production worldwide. There is an urgent need to integrate buildings with smart grid operation to accommodate the needs of flexible load controls due to the increasing of renewable energy resources. In the imminent future, smart buildings can contribute to grid stability by changing their overall demand patterns in response to grid operations. Meanwhile, building thermal energy consumption is also maintained by building operators to satisfy occupants' thermal comforts. However, explicit large-scale demonstrations based on a simulation platform that integrates building occupancy, building physics, and grid physics at community level have not been explored. This study develops an occupancy behavior driven BtG optimization platform that can simulate, predict and optimize indoor temperature and energy consumption of buildings, generator setpoint and deviation while maintaining acceptable grid frequency. Authors have tested the framework on two standard power networks. The results show that the integrated framework can provide potential cost savings up to 60% comparing with the decoupled operation.

Highlights:

- Development of a centralized occupancy-based Buildings-to-grid Model Predictive Control (MPC) framework.
- Simulation on randomized building clusters and standard IEEE grid systems.
- Findings show 50%-61% cost reduction for BtG integration.

	Occupancy Predictor
p	Transition probability
α	Distribution weight factor
β	Smooth factor
s	Occupancy state
	Building System Physics
C	Thermal capacity
R	Thermal resistance
T_{wall}	Wall temperature
T_{zone}	Zone temperature
Q	Heat gain
Q_{sol}	Solar heat
Q_{int}	Internal heat
Q_{hvac}	HVAC cooling
η	HVAC coefficient of performance
$\mathbf{x_b}$	Building temperature states
$\mathbf{u_b}$	Building control inputs
$\mathbf{w_b}$	Building disturbances
	Grid System Physics
θ	Bus voltage angle
D	Damping coefficient
M	Inertia coefficient
P	Power
P_m	Mechanical power input
P_e	Electricity demand load
P_{misc}	Miscellaneous building load
P_{hvac}	Building HVAC load
ω	Bus frequency
$\mathbf{x_g}$	Grid states
$\mathbf{u_g}$	Building load to grid
$\mathbf{u_m}$	Controllable mechanical powers to grid
$\mathbf{w}_g$	Grid disturbances
	BtG MPC
C	Building cost as the grid price
ϵ	Slack relaxation based on occupancy prediction
a	Quadratic generator cost
b	Linear generator cost
f	Quadratic frequency cost

1. Introduction

In response to dramatic growth of power demand, use of renewable energy, and critical risk of building power blackouts, smart buildings and smart grid that can communicate with each other have more benefits for building management and power operation. Recent reports from the U.S. Department of Energy show that (1) buildings consume 74% of electricity produced by the grid in

the U.S.; (2) buildings are able to reduce their consumption by 20-38% using advanced sensors and controls; and (3) 90% of the commercial buildings can be aggregated to connect to the grid [1-3]. Hence, it is necessary to investigate and understand the coupling between buildings and grids for optimizing the energy consumptions and the operation costs.

1.1 Building MPCs and research gaps

Model predictive control (MPC) is one real-time control algorithm that connects buildings to grids, thereby establishing a computational framework to co-optimize the decisions of building and grid operators. Studies interoperating buildings and grids using MPC for demand response are presented in recent literature overviews [4-5]. For commercial buildings, a bi-level MPC optimization is designed to control the voltage and current in a distribution grid while building zonal models are integrated [6]. The study provides a framework comprising mathematical models of commercial buildings and the distribution grid. Commercial building MPC or model-based supervisory control can also regulate the building power frequency by controlling the fan power consumption, the chiller operation sequence, and the air-side ventilation system [7-8]. Those studies treat buildings as fast demand side resources to reduce frequency deviations in grid operations. Customized designs of the model-based controllers can further provide ancillary services to the grid [9-10]. One study optimizes the chiller to respond fast to the demand response signal [9]. Another study investigates the ancillary service capacity under optimal HVAC usages [10]. For residential buildings, grid-aware MPCs are carried out to reduce the costs of smart homes by using energy storage, appliance scheduling, electric vehicles, and distributed generation units [11-15]. These studies usually focus microgrid or small-scale interactions between buildings and grids. The majority of the aforementioned research shows significant energy savings given different building systems with no account for larger scale simulations of building clusters.

One recent study [16] expands the current research scope by using a detailed physics model of a building cluster for a smart grid optimization. Although large-scale building aggregation is performed, the models of electricity generation and renewable energy source are oversimplified with no gird physics. Hence, the grid frequency and power flow transmission cannot be regulated. Furthermore, how to achieve the optimal control for hundreds of grid-aware commercial buildings is not demonstrated, especially considering the significant time-scale discrepancy between building demand change (minutes to hours) and grid power supply (milliseconds to seconds). Therefore, an explicit simulation of the building dynamics, grid dynamics, generator capacity, and BtG operation cost from a large-scale control strategy is a critical research question not fully addressed yet [17].

1.2 Missing of the occupant behavior

Another key component missing in the large scale BtG integration is the building occupancy. Humans spend more than 90% of their time in buildings, and the buildings themselves are designed to provide a comfortable indoor environment for occupants [18]. The human-building interactions, such as usage of lighting and air conditioning, consume around one quarter to half of the total amount of commercial building energy [19]. On the other hand, office workers arrive and leave the workspaces regularly according to schedules. The stochastic occupancy pattern can be detected easily by occupancy sensors, which are commonly installed in today's smart buildings [20]. Therefore, it is a natural idea to utilize the occupancy information to reduce the energy consumption caused by human-building interaction while maintaining occupants' comfort [21]. Typical occupancy schedules used to optimize building operations are conservative on energy savings [22]. Larger savings with stable comfort satisfactions can be further achieved through learning and prediction of the office occupancy [23].

Current research has found a range of strategies to predict and utilize the occupancy in single building control [24-26]. The optimization of air conditioning systems is demonstrated through building MPCs using the hidden Markov chain to predict the occupant numbers [27]. First order Markov chain (MC) is another popular method that can provide online occupancy predictions. One study trains a MC in a moving window for an occupancy driven MPC of commercial buildings [28]. The occupied periods are found by aggregated predictions of the occupancy models. The occupied periods' setpoint temperature of the air conditioning is reset from the high temperatures of unoccupied periods. A similar example is shown by penalizing the discomfort index during occupancy. Occupied periods are estimated using a MC that is trained through Bayesian inference [29]. Savings are shown by preheating, no conditioning at vacancies, and suppressing the peak demands. A more detailed description of the Markov model will be introduced in the following section of methodology. Other occupancy models have also been extensively explored for building simulations, such as random sampling [30], machine learning [31], data mining [32] and agent-based models [33]. However, most studies focus on the occupancy-buildings coupling are still ignoring the complete picture to associate occupancy, buildings, and grids together [34-36]. How those occupancy-based MPCs effect the aggregation of building demand and influence the optimization of grid operation remains largely unknown.

1.3 Innovations of the study

Based on the aforementioned review, the study addresses the following research gaps for a large scale BtG integration: 1) lack of investigation of advanced control strategies for the integration of occupancy, buildings and grid, and 2) lack of evaluation of the occupancy impact on the individual thermal comfort and energy savings. Three integration approaches are proposed and studied as: 1) a decoupled buildings and grid optimization (**DB&G**), 2) a centralized Buildings-to-Grid

integration (**BtG**), and 3) a centralized occupancy-based BtG integration (**OBtG**). **DB&G** introduces on/off controls for buildings and model predictive control (MPC) for the grid. **BtG** introduces an innovative MPC to control the buildings and grid simultaneously with the time discrepancy between the buildings and grid operations. **OBtG** integrates occupancy predictions to improve energy efficiency by maintaining the thermal comfort at the occupied periods while reducing energy consumption when buildings are not occupied. **BtG** and **OBtG** are used to generate high-level local control operations for both building systems and grid generators such that the overall performance is optimized in terms of power network stability, energy savings, and comfort satisfactions. The contributions of this study are: 1) a new online occupancy predictor to predict the occupancy at the building level; 2) complete high-level integrations among occupancy, buildings, and grid with system-level objectives and constraints; and 3) a three-level design of the buildings-to-grid integrations to address the operation time-scale discrepancy and the large-scale computational cost. The paper is organized as follows: Section 2 presents the overall methodology including occupancy model, building physics, grid dynamics, and formulation of the three integration approaches; Section 3 discusses simulation results; and Section 4 concludes this paper with open research problems and future studies.

2. Methodology

The final centralized **OBtG** approach is developed to integrate the systems of occupancy, buildings, and grid, as shown in Figure 1. The objective is to develop an explicit mathematical MPC framework for large-scale buildings-to-grid integration with building occupancy behavior interactions. The MPC structure uses the computationally efficient, convex quadratic programming for optimization, whereby the control laws for the slower (buildings) and faster (grid) operations are jointly computed. As shown by Figure 1, the time-steps of the latter (grid) are

nested in the time-steps of the former (buildings) through building variables u_b and u_s, while the system states (x_b and x_g) and all controllable variables (u_b, u_g, and Δu_g) jointly evolve according to the coupling between the physics models of buildings and grids. Non-controllable inputs including disturbances and constraints that are imposed to the MPC are assumed to be measurable, such as local weather from on-site weather stations. The model formulations and system physics are illustrated in Sections 2.1, 2.2 and 2.3 for building occupancy, building physics, and grid physics respectively. The details of BtG integration are described in Section 2.4.

2.1 Modeling of Occupancy

Three basic types of occupancy models exist in prior studies [37]. Type I is the occupancy status at a space level, addressing whether or not a space is occupied at a particular time. Type II is the number of occupants at a space level, addressing how many occupants are in the space at a particular time. Type III is the occupant tracking, addressing individual movement and behavior tracking. In this study, the status of building occupants influences the building state constraints (zone temperature). Thus, Type I information, the occupancy states of presence and absence, are enough for control purposes.

A modified occupancy approach is integrated with building MPC based on the authors' recent work [38]. The modeling technique develops a first order Markov chain with a moving training window driven by change-point detection. Define a Markov chain given by the time sequence $x_1, x_2, ..., x_k$ ending at time step k, where at each time step, the Markov chain can take values from the states $\{s_1, s_2\}$ representing binary occupancy (i.e., presence or absence). The chance of the state transition from s_i to s_j at time step $k+1$ is decided by the transition probability at time step k defined as

$$p_k^{ij} = p(x_{k+1} = s_j | x_k = s_i) \tag{1}$$

The transition probabilities between states for more than one step are more easily calculated using a transition matrix. Let the transition matrix $\mathbf{P}_k = (p_k)_{i,j}$ denote the matrix where the element indexed by (i, j) represents the probability defined in Eq. (1).

The transition matrix $\mathbf{P}_k$ is trained within a moving optimal window. Define a moving window $w = \{x_t, x_{t+1}, ..., x_s\}$ where $0 \le t < s \le k$ holds for the Markov chain prediction at time step $k+1$. Within the window, there are n_{ij} transitions from s_i to s_j among all transitions from s_i to s_l. Then, the probability of transition from s_i to s_j is estimated as

$$\hat{p}_{ij} = \frac{n_{ij} + \alpha}{\sum_{l=0}^{1} (n_{il} + \alpha)} \tag{2}$$

where $\hat{p}_{ij}$ is the estimated transition probability from state s_i to s_j and α is a smoothing factor. A properly defined smooth factor could enforce the likelihood of occupancy changes during the dramatic increase of occupancy presence at the morning ramp-up, varied occupancy at the lunch break, and dramatic decrease of occupancy presence at the evening ramp-down. The authors note that this study has a binary inhomogeneous occupancy chain (e.g. presence and absence). Based on office occupancy patterns, there are periods of very low or zero transition probabilities, defined as sink transitions [39]. A small smooth factor is preferred in order not to force the unlikely occupancy changes to be happening during those sink periods. The authors defined the factor as a time related step function of 0, 0.05, and 0.1, where empirical rules are used to decide the specific value at certain time.

The Markov occupancy model is going to be integrated into a rolling window MPC. Assuming a case that the building MPC is rolling at 15 minutes ahead during one test day, there are a total of 96 transition matrices that need to be updated for each optimized step of MPC since one day has 96 intervals of 15 minutes. For each transition matrix, the Markov chain's transition probabilities are trained within an optimal window before each of the predicted time step. The period of the training window is decided by the changing point of the occupancy presence rate based on a daily occupancy profile, as shown in the hypothetical MPC of Figure 2. Binary occupancy data during the same time period in this training window ("training window" in Figure 2) for each day of the ten most recent historical days are the training data for the transition probabilities in Eq. (1). To overcome the uncertainties from the limited training size, a modified bootstrap sampling strategy is used as follows:

1) Randomly sample nine days from the training data and apply Eq. (2) to get one bootstrap transition matrix;
2) Resample ten times using the procedure above; and
3) Calculate the average values of the ten bootstrap transition matrices.

The details of the changing-point detection are described next. Let $D = \{d_1,...,d_{96\times z}\}$ represent the selected data from z days before the time step to be predicted. Here, if the occupancy presence state to be predicted is in a working day, the selection of D only contains the available profiles of z working days. Additionally, d is binary state that represents the presence and absence as 1 and 0, respectively. A discrete profile of the presence probability [38] is generated by

$$P_m = \frac{\sum_{j=1}^{z}(\lambda^{z-j} \cdot d_{(j-1)\times 96+m})}{z} \tag{3}$$

where $1 \le m \le 96$ if the occupancy data is in 15-minute scale and λ is an exponential forgetting factor, which is smaller than one. Again, the building MPC is performing rolling window optimization and new occupancy information is updated through an ongoing measurement. During the continuous updates of the occupancy presence rates of Eq. (3), the forgetting factor gives more weight on the recent occupancy presence information rather than the old one.

The authors assume that a change of the optimal training window length should happen based on the change points of the presence rate calculated by Eq. (3). The change detection algorithm in this study uses relative density-ratio estimation with the Pearson divergence as a measure to score the possible change points. For a subsample distribution $p(m)$ selected from the sample distribution $p(n)$, the symmetric divergence score [40] is defined as

$$S=\int p_\beta(m)\left[\frac{p(n)}{p_\beta(m)}-1\right]^2 d(m)+\int p(n)\left[\frac{p_\beta(m)}{p(n)}-1\right]^2 d(n) \tag{4}$$

where S is the score, and $p_\beta(m)=\beta p(n)+(1-\beta)p(m)$. Notice that $p(m)$ and $p(n)$ are the preselected probability density functions of the corresponding variables, and the factor β is a density ratio. For the example of Figure 2, the day file contains 96 occupancy rates in 15-minute resolution which indicates the sample n in Eq. (4) follows a preselected Gaussian distribution $p(n)$ fitted by 96 presence probabilities. The change point is detected by using a sliding window size of 12 intervals (3-hour data) which indicates a preselected Gaussian distribution $p(m)$ fitted by 12 presence probabilities for this subsample m in Eq. (4). The sliding window moves forward from the beginning of the day until the end of the day and then resamples backwards from the end to the beginning again. The symmetric score is calculated by the summation of the forward sliding

and backward sliding scores S using Eq. (4). The MATLAB toolbox developed by Liu is used [40].

In this study, the occupancy number of each building for **OBtG** optimization is generated from an occupancy simulator developed by Lawrence Berkeley National Laboratory (LBNL) [41]. The LBNL simulator gives detailed occupancy number simulation at the building level for a selected simulation period, which provides Type II occupancy information. A filter is used to pass the simulated occupancy number to occupancy presence which is the Type I occupancy information needed in this study. The passing threshold is 30% of the max number observed in the simulated data for each building respectively. The presence rate is then calculated based on Eq. (3) for each building again. As shown in Figure 2, the individual optimized windows are decided using Eq. (4). The transition matrices are updated using Eq. (2) afterwards. Prediction for the occupancy presence and absence is made based on all updated transition matrices accordingly during the building MPC.

2.2 Modeling of Building Dynamics

The total electricity load of a commercial building is composed by two parts: base power demand and controllable power demand. Electrical load of lighting, electrical equipment, and other appliances are the base demand, which can be modelled and predicted by operation schedules. In contrast, electricity load of HVAC systems is a controllable load which is possible to be altered by adjusting building indoor temperature setpoints. Here, as the first attempt for a large-scale buildings-to-grid integration within a community, only an ideal cooling system for each building is modeled where the optimal control variable is temperature set-point. It is assumed that a decoupled or distributed PID control strategy could achieve the optimized setpoint at the lower

level (air handling unit, roof top units, etc.), which has been demonstrated in a few prior research studies [42-44].

The optimal HVAC demand is predicted through the control of the building physics model, and specifically, the thermal resistance and capacitance (RC) network. The lowest order network, namely 1R-1C, is limited to a well-insulated room with fewer heat sources [45]. The high order network, 3R-2C or even higher, provides accurate estimations of the temperature response in retail stores, campus buildings, and skyscrapers [46-49]. However, the 3R-2C model is computationally complex for modeling all zones within hundreds or thousands of buildings within a community. In this study, a 2R-1C thermal network model is developed which only has two temperature states, namely, building zone temperature T_{zone} and building wall structure temperature T_{wall} for each building, as depicted in Figure 3.

From Figure 3, the temperature states T_{wall} and $T_{\text{zone,}}$ of the "super-zone" are given by

$$\begin{aligned} C\dot{T}_{wall} &= \frac{T_{amb} - T_{wall}}{R_2} + \frac{T_{zone} - T_{wall}}{R_1} + Q_{sol} \\ C_{zone}\dot{T}_{zone} &= \frac{T_{wall} - T_{zone}}{R_1} + \frac{T_{amb} - T_{zone}}{R_{win}} + Q_{\text{int}} + Q_{hvac} \end{aligned} \tag{5}$$

where R_1 , R_2 , R_{win} are the aggregated thermal resistances of the exterior structure, interior structure, and window; C_{zone}, and C are the aggregated thermal capacitances of the zone and walls' structure; T_{amb} , T_{wall} , and T_{zone} are the ambient exterior temperature, the walls' structure temperature, and the aggregated zone temperature; and Q_{sol} , Q_{int} , and Q_{hvac} are the solar disturbance heat gain, the internal heat gain from the miscellaneous power consumption, and the HVAC load from the conditioning power consumption.

Considering building clusters comprising hundreds of buildings, the state-space formulation is expressed as

$$\dot{\mathbf{x}}_{\mathbf{b}} = \mathbf{A}_{\mathbf{b}}\mathbf{x}_{\mathbf{b}} + \mathbf{B}_{\mathbf{ub}}\mathbf{u}_{\mathbf{b}} + \mathbf{B}_{\mathbf{wb}}\mathbf{w}_{\mathbf{b}} \tag{6}$$

where $\mathbf{x}_{\mathbf{b}}$ are building temperature states, $\mathbf{u}_{\mathbf{b}} = \eta \mathbf{Q}_{hvac} = \mathbf{P}_{hvac}$ is the building air conditioning control input and η is the coefficient of performance of the HVAC systems, $\mathbf{w}_{\mathbf{b}}$ are the building disturbances, $\mathbf{A}_{\mathbf{b}}$ is the coefficient matrix of the building states, $\mathbf{B}_{\mathbf{ub}}$ is the coefficient matrix of the control inputs, and $\mathbf{B}_{\mathbf{wb}}$ is the coefficient matrix of the building disturbances.

2.3 Modeling of Grid Dynamics

The electricity grid has three functions: generation, transmission, and distribution of electricity power. The connection points between the grid transmission lines and the generators are grid buses. A typical IEEE test grid with multiple buses [51] is illustrated in Figure 4, which is one test case of this study. Three large generators are connected to grid through the three buses at generation sides (Buses 4, 6, and 8). The power flows through the transmission lines to distribution buses (Bus 5, 7, and 9) and connected to demand-side building clusters. It is also noticed that each generation bus is connected to two distribution buses in the example of Figure 4. There are generally different costs for generators and buildings at distribution buses. An optimal power flow problem can be formulated to minimize the overall system cost.

Several models of grid systems exist, with different accuracy and computational complexity [51-52]. Considering the example in Figure 4, the total electrical power injection S_k into bus k can be expressed as

$$S_k = P_k - iQ_k \tag{7}$$

where i is imaginary number, P_k is the active power injection and Q_k is the reactive power injection. It is also noticed that the power variable is a complex number. Physical considerations dictate the following complex parameter for the transmission line connecting bus k and bus j

$$Y_{kj} = g_{kj} - ib_{kj} \tag{8}$$

where Y_{kj} is the admittance of the transmission line connecting bus node k and bus node j, g_{kj} is the conductance of the transmission line, and b_{kj} is the susceptance of the transmission line. The real and reactive power injections into bus *k* become power flows on the transmission lines. Using Ohm's Law, the real and reactive power flows on the line connecting buses *k* and *j* are expressed as

$$\begin{aligned} P_{kj} &= V_k^2 g_{kj} - V_k V_j [g_{kj} \cos(\theta_k - \theta_j) - b_{kj} \sin(\theta_k - \theta_j)] \\ Q_{kj} &= V_k^2 b_{kj} - V_k V_j [g_{kj} \sin(\theta_k - \theta_j) + b_{kj} \cos(\theta_k - \theta_j)] \end{aligned} \tag{9}$$

where V_k, V_j, θ_k, θ_j are the voltage magnitudes (kV) and voltage angles of buses k and j respectively.

However, the accurate power flow equations in (9) are computationally challenging in the scope of large-scale BtG integration, because they are nonlinear and nonconvex. A simplified power flow model can be alternatively formulated under reasonable assumptions that tend to hold in practice [53]. These assumptions enable the linearization of Eq. (9):

1) The resistance for each branch of the transmission line is negligible compared to the reactance and therefore can be set to zero, which leads to $g_{kj} = 0$.
2) The voltage magnitudes at all buses are (approximately) equal to their base (nominal) values.

3) The voltage angle differences across each transmission lines are small, and thus $\cos(\theta_k - \theta_j) \approx 1$ and $\sin(\theta_k - \theta_j) \approx \theta_k - \theta_j$ hold.

By substituting the assumptions into Eq. (9), the power flow model is reduced to

$$P_{km} = V_o^2 b_{km}(\theta_k - \theta_j) \tag{10}$$

where V_o is the base (nominal) voltage magnitude (kV). The parameter V_o can be further eliminated by scaling it to a dimensionless per unit (p.u.) quantity so that $|V_o| \approx 1 p.u.$.

The generators connected to the grid are normally synchronous machines with rotors that spin at synchronous speed. The dynamics of the mechanical power transfer to electricity power by the generators are modeled by the rotational counterpart of Newton's law

$$J\ddot{\theta} = T^m - T^e \tag{11}$$

where θ is the rotor voltage angle, J is the moment of inertia, T^m is the mechanical torque input to the generator from the turbine, and T^e is the electrical torque on the generator rotor. The electrical torque corresponds to the electrical power that the generator provides. This electrical power serves any load attached to the generator bus or is converted to power flows on the lines leaving the generator bus. The first derivative $\dot{\theta}$ is the angular frequency ω. The left-hand side of Eq. (11) is typically augmented by a damping torque that is proportional to $\dot{\theta}$. The nominal value of the angular frequency corresponds to the electrical frequency of 60 Hz that is used in North America's grid. Supposing that the angular frequency remains close to its nominal value, the mechanical and electrical torques in Eq. (11) are converted to powers by multiplying with the nominal angular frequency, which results in the *swing equation* for bus k

$$M_k\ddot{\theta}_k + D_k\dot{\theta}_k = P_k^m - P_k^e - \sum_{j=1}^{n} P_{kj} \tag{12}$$

where n is the number of buses, θ_k is the bus voltage angle, M_k is the inertia coefficient, D_k is the damping coefficient, P_k^m is the mechanical power input to generator, P_k^e is the electricity load demand at bus k, P_{kj} is the power flow from bus k to bus j, and $\sum_{j=1}^{n} P_{kj}$ is the cumulative power flow over line (k,j), and n is the number of buses in the network. The power flow P_{kj} in Eq. (12) is given by Eq. (10)

$$P_{kj} = b_{kj}(\theta_k - \theta_j) \tag{13}$$

where $P_{kj} = 0$ if there is no line connecting buses k and j. The electricity load P_k^e at the k th bus of Eq. (12) can be decomposed into three components as

$$P_k^e = E_k\dot{\theta}_k + P_k^i + \sum_{l=1}^{L_k} P_{\{k,l\}}^b \tag{14}$$

where $E_k\dot{\theta}_k$ is the frequency-sensitive uncontrollable load, P_k^i is the frequency-insensitive load, P^b is individual building power load, and $\sum_{l=1}^{L_k} P_{\{k,l\}}^b$ is the cumulative power demand from the buildings that are connected to the k th bus, and the total number of buildings connected to bus k is L_k.

The individual building power load in Eq. (14) is defined as

$$P^b = P_{hvac} + P_{misc} \tag{15}$$

where P_{hvac} is the HVAC load that can participate in frequency regulation and was introduces in Section 2.2, and P_{misc} represents the miscellaneous loads with no potential to contribute to frequency regulation in this study.

By combining Eq. (12)-(15), the authors obtain a governing equation by letting $\dot{\theta}_k = \omega_k$ for the grid system as follows

$$M_k \dot{\omega}_k = -(D_k + E_k)\omega_k + P_k^m + \sum_{j=1}^{n} b_{kj}(\theta_k - \theta_j) - P_k^i - \sum_{l=1}^{L_k}(P_{hvac} + P_{misc}) \tag{16}$$

A linear state-space representation of the grid system can be derived based on Eq. (16) as

$$\mathbf{A_e}\dot{\mathbf{x}}_\mathbf{g} = \mathbf{A_g}\mathbf{x_g} + \mathbf{A_{ub}}\mathbf{u_b} + \mathbf{B_m}\mathbf{u_m} + \mathbf{B_{wg}}\mathbf{w_g} \tag{17}$$

where $\mathbf{x_g}$ is the grid state, $\mathbf{u_b}$ is the building load to grid which was introduced in Eq. (6), $\mathbf{u_m}$ is the controllable mechanical power to grid, and $\mathbf{w_g}$ is the frequency-insensitive grid load including grid base load and the building miscellaneous load.

2.4 Modeling of Buildings-to-Grid Integration

The objective of the BtG framework in this study is to generate high level control setpoints for buildings and power generators such that the overall performance is optimized—in terms of system stability, energy savings, and cost reductions. The dynamics in Eq. (5) and Eq. (16) clearly operate at two different time-scales. Model predictive control (MPC) is developed to control the physics responses of these systems based on Eq. (6) and (17), and the time discrepancies are solved via constraints in the optimal problem formulations. In order to formulate the BtG framework, both MPCs for building and grid are developed. The building only MPC is introduced at Section 2.4.1. The grid only MPC is introduced at Section. 2.4.2. The BtG integrated MPC is presented at Section 2.4.3.

2.4.1 Building MPC

The building MPC discussed here is designed for building cluster only without considering the grid dynamics. The uniqueness of the large-scale buildings-to-grid integration is that a cluster of

buildings needs to be simulated and controlled simultaneously. The canonical linear form of the building MPC during the prediction horizon $[0,t_p]$ for the dynamics defined in Eq. (6) is derived as

$$\begin{aligned} &\min_{\mathbf{U_b}} \int_{\mathbf{0}}^{\mathbf{t_p}} (\mathbf{c}^{\mathbf{T}}\mathbf{u_b})dt \\ \text{s.t.}\quad &\dot{\mathbf{x}}_\mathbf{b} = \mathbf{A_b}\mathbf{x_b} + \mathbf{B_{ub}}\mathbf{u_b} + \mathbf{B_{wb}}\mathbf{w_b} \\ &\mathbf{x_b^{min}} \le \mathbf{x_b} \le \mathbf{x_b^{max}} + \boldsymbol{\varepsilon}_{\mathbf{ub}}(O) \\ &\mathbf{u_b^{min}} \le \mathbf{u_b} \le \mathbf{u_b^{max}} \end{aligned} \tag{18}$$

where $\mathbf{c}$ refers to the cost of building power consumption based on the grid price ($/KWh), $\mathbf{u_b^{min}}$, $\mathbf{u_b^{max}}$, $\mathbf{x_b^{min}}$, $\mathbf{x_b^{max}}$ are the minimum and maximum constraints on the control inputs $\mathbf{u_b}$ or the building states $\mathbf{x_b}$, and other parameter notations are same as in Eq. (6).

An occupancy-based MPC is additionally developed to evaluate the impacts of occupancy and enable deeper energy savings. The authors introduce an occupancy-based slack relaxation on the building states' constraints in Eq. (18). The occupancy information such as presence and absence is simulated and predicted based on the model developed in Section 2.1. It is designed to focus on the occupancy status at the whole building level. For example, the occupancy model predicts the lunch break as absence during certain time periods if the aggregated training data show a majority of the people leaving the offices for lunch. Hence, the upper bounds on indoor temperature increase from $\mathbf{x_b^{max}}$ to $\mathbf{x_b^{max}} + \boldsymbol{\varepsilon}_{\mathbf{ub}}(O)$ during cooling condition. Function $\boldsymbol{\varepsilon}_{\mathbf{ub}}(O)$ is the occupancy-based slack relaxation function, and O is the binary occupancy state at optimized time step t. The relaxation function in Eq. (18) is defined as

$$\varepsilon_{\mathbf{ub}}(O(t)) = \begin{cases} \Delta T & if \quad 0 < \Gamma(O) < 1 \\ \min\{\Delta T, \mathbf{x_b}(t-1) - \mathbf{x_b^{max}}(t-1) - \boldsymbol{\varepsilon}_{\mathbf{ub}}(O(t-1))\} & if \quad \Gamma(O) > 1 \\ 0 & if \quad \Gamma(O) = 1 \end{cases} \tag{19}$$

where ΔT is the constraint adjustment threshold for building states (1-2 °C) , and conditional function Γ is defined as $\Gamma(O) = O + \max\{0, \mathbf{x_b}(t-1) - \mathbf{x_b^{max}}(t-1) - \boldsymbol{\varepsilon}_{\mathbf{ub}}(O(t-1))\}$ where $\mathbf{x_b}$ is the building states vector and $\mathbf{x_b^{max}}$ is the predefined upper bound on building states. This empirical derived relaxation formulation is designed to balance the feasibility of the numerical solver and the savings of the optimal solution.

2.4.2 Grid MPC

The grid MPC in this study optimizes the power generation costs as well as the cost of frequency deviations. It is assumed that each generator has variable and fixed costs of production while transmission losses are negligible. Simplified cost optimization is developed without considerations of the no-load operation, startup or shutdown costs, and ramping constraints. Let $\mathbf{u_m}$ in Eq. (17) to be $\mathbf{u_m} = \bar{\mathbf{u}}_\mathbf{m} + \boldsymbol{\Delta}\mathbf{u_m}$ where $\boldsymbol{\Delta}\mathbf{u_m}$ is the additional adjustments on the mechanical power setpoints $\bar{\mathbf{u}}_\mathbf{m}$ of Eq. (20), the total cost function of the generators takes the form as

$$\int_0^t (\bar{\mathbf{u}}_\mathbf{m}{}^\mathbf{T} \mathbf{A}_{\bar{\mathbf{u}}} \bar{\mathbf{u}}_\mathbf{m} + \mathbf{B}_{\bar{\mathbf{u}}}^\mathbf{T} \bar{\mathbf{u}}_\mathbf{m} + c\boldsymbol{\Delta}\mathbf{u}_\mathbf{m}^\mathbf{T} \mathbf{A}_{\boldsymbol{\Delta}\mathbf{u}} \boldsymbol{\Delta}\mathbf{u}_\mathbf{m} + c\mathbf{B}_{\boldsymbol{\Delta}\mathbf{u}}^\mathbf{T} \boldsymbol{\Delta}\mathbf{u}_\mathbf{m} + \mathbf{x}_\mathbf{g}{}^\mathbf{T} \mathbf{F}_\boldsymbol{\omega} \mathbf{x}_\mathbf{g}) dt \tag{20}$$

where $\bar{\mathbf{u}}_\mathbf{m} = \begin{bmatrix} \bar{u}_1 \\ \vdots \\ \bar{u}_{n_g} \end{bmatrix}$, $\mathbf{A}_{\bar{\mathbf{u}}} = \begin{bmatrix} a_1 & & \\ & \ddots & \\ & & a_{n_g} \end{bmatrix}$ has units of \$/MW^{2}h, and $\mathbf{B}_{\bar{\mathbf{u}}} = \begin{bmatrix} b_1 \\ \vdots \\ b_{n_g} \end{bmatrix}$ has units of \$/MWh, $\boldsymbol{\Delta}\mathbf{u_m}$, $\mathbf{A}_{\boldsymbol{\Delta}\mathbf{u}}$, $\mathbf{B}_{\boldsymbol{\Delta}\mathbf{u}}$ are all defined similarly to $\bar{\mathbf{u}}_\mathbf{m}$, $\mathbf{A}_{\bar{\mathbf{u}}}$, and $\mathbf{B}_{\bar{\mathbf{u}}}$, $\mathbf{x_g}$ is the grid state in Eq. (17), c is the penalty factor on generators' adjustments, and $\mathbf{F}_\boldsymbol{\omega} = diag(0 \quad f_g \quad \cdots \quad 0 \quad f_g)_{2n \times 2n}$ is a diagonal matrix with the frequency deviation penalty f_g for the frequency ω in $\mathbf{x_g}$.

The canonical linear form of the grid only MPC during the prediction horizon $[0,t]$ combining Eq. (17) and Eq. (20) is written as

$$\begin{aligned} \min_{U_b} \quad & \int_0^t (\bar{\mathbf{u}}_\mathbf{m}{}^\mathrm{T} \mathbf{A}_{\bar{\mathbf{u}}} \bar{\mathbf{u}}_\mathbf{m} + \mathbf{B}_{\bar{\mathbf{u}}}^\mathrm{T} \bar{\mathbf{u}}_\mathbf{m} + c\Delta\mathbf{u}_\mathbf{m}^\mathrm{T} \mathbf{A}_{\Delta\mathbf{u}} \Delta\mathbf{u}_\mathbf{m} + c\mathbf{B}_{\Delta\mathbf{u}}^\mathrm{T} \Delta\mathbf{u}_\mathbf{m} + \mathbf{x}_\mathbf{g}{}^\mathrm{T} \mathbf{F}_\omega \mathbf{x}_\mathbf{g}) dt \\ \text{s.t.} \quad & \mathbf{A}_\mathbf{e} \dot{\mathbf{x}}_\mathbf{g} = \mathbf{A}_\mathbf{g} \mathbf{x}_\mathbf{g} + \mathbf{A}_{\mathbf{ub}} \mathbf{u}_\mathbf{b} + \mathbf{B}_\mathbf{m} (\bar{\mathbf{u}}_\mathbf{m} + \Delta\mathbf{u}_m) + \mathbf{B}_{\mathbf{wg}} \mathbf{w}_\mathbf{g} \\ & \Delta\mathbf{u}_\mathbf{m}^{\mathbf{min}} \le \Delta\mathbf{u}_\mathbf{m} \le \Delta\mathbf{u}_\mathbf{m}^{\mathbf{max}} \\ & \bar{\mathbf{u}}_\mathbf{m}^{\mathbf{min}} \le \bar{\mathbf{u}}_\mathbf{m} \le \bar{\mathbf{u}}_\mathbf{m}^{\mathbf{max}} \\ & \mathbf{x}_\mathbf{g}^{\mathbf{min}} \le \mathbf{x}_\mathbf{g} \le \mathbf{x}_\mathbf{g}^{\mathbf{max}} \\ & \mathbf{A}_\mathbf{f} \mathbf{x}_\mathbf{g} \le \mathbf{F}_{\mathbf{neq}} \end{aligned} \tag{21}$$

where $\mathbf{u}_\mathbf{b}$ is introduced in Eq. (6) and $\Delta\mathbf{u}_\mathbf{m}^{\mathbf{min}}, \Delta\mathbf{u}_\mathbf{m}^{\mathbf{max}}, \bar{\mathbf{u}}_\mathbf{m}^{\mathbf{min}}, \bar{\mathbf{u}}_\mathbf{m}^{\mathbf{max}}, \mathbf{x}_\mathbf{g}^{\mathbf{min}}, \mathbf{x}_\mathbf{g}^{\mathbf{max}}$ are the minimum and maximum constraints for the corresponding building control variables and grid system states. Other parameter notations are the same as Eq. (17). The authors also introduce an inequality constraint $\mathbf{A}_\mathbf{f} \mathbf{x}_\mathbf{g} \le \mathbf{F}_{\mathbf{neq}}$ to enforce the thermal limits on the transmission lines.

2.4.3 Buildings-to-grid MPC

The integration of the two MPCs from Sections 2.4.1 and 2.4.2 can formulate a centralized MPC that optimizes the cost of the buildings and grid simultaneously. Given the case of large-scale BtG MPC, the authors first limit the rolling window of MPC at 15-minute ahead prediction for each rolling step. The rolling step is 10 seconds to match the normal grid operation. During each period of 10 seconds, the MPC optimized control trajectories are calculated for both building and grid for 15 minutes ahead. However, it is not necessary to optimize the building control at 10-second interval for each MPC due to the slow responses of the building thermal states. The authors propose a three-level hierarchical MPC that addresses the issues of the operation time discrepancy between buildings and grid to reduce the computational complexity, where the control variables are described next and are depicted in Figure 5.

(1) Level 1: The first level of MPC is only used exactly every 15 mins. In other words, only the rolling steps that occur every 15 mins use level-one MPC to optimize the three control variables of Eq. (18) and Eq. (21): the building HVAC power $\mathbf{u_b}$, the mechanical power setpoint $\bar{\mathbf{u}}_\mathbf{m}$ for generator, and the adjustment of the mechanical power setpoint $\mathbf{\Delta u_m}$. For the example of Figure 5, one generator's setpoint $\bar{u}_m$, one generator's adjustment Δu_m, and one building HVAC power u_b are going to be optimized simultaneously every 15 mins.

(2) Level 2: Continuing to roll the MPCs in between the intervals of 5 mins, the authors design a level-two MPC based on the optimized building HVAC power $\mathbf{u_b}$ and the optimized mechanical power setpoints $\bar{\mathbf{u}}_\mathbf{m}$ from the previous MPCs. Only the adjustments $\mathbf{\Delta u_m}$ are optimized every 10 secs. Using the example in Figure 5 again, the rolling steps from 10 secs to 4 mins and 50 secs have constant $\bar{u}_m$ and u_b at all the times for each rolling MPC while Δu_m is optimized during each MPC. The values of $\bar{u}_m$ and u_b are optimized values from the first level-one MPC.

(3) Level 3: If the rolling MPC is exactly every 5 mins, a level-three MPC is designed that the building HVAC power $\mathbf{u_b}$ is updated for next 5 minutes. For the example in Figure 5, the MPC at the 5- and 10-minute time steps are updated. Meanwhile, for periods between 5 to 10 mins, and 10 to 15 mins, the level-two MPCs are using the updated u_b, the building HVAC power, from level-three MPCs. A similar strategy is applied to all future steps of integrated MPC.

For each level of the MPC, a quadratic programming formulation from Eq. (18) and Eq. (21) is developed as

$$\begin{aligned} \min\ & \mathbf{x}^{\mathrm{T}}\mathbf{H}_{\mathbf{x}}\mathbf{x} + \mathbf{F}_{\mathbf{x}}^{\mathrm{T}}\mathbf{x} \\ \text{s.t.}\ & \mathbf{A}_{\mathbf{eq}}\mathbf{x} = \mathbf{b}_{\mathbf{eq}} \\ & \mathbf{A}_{\mathbf{ineq}}\mathbf{x} \le \mathbf{b}_{\mathbf{ineq}} \\ & \mathbf{x}^{\mathbf{min}} \le \mathbf{x} \le \mathbf{x}^{\mathbf{max}} \end{aligned} \tag{22}$$

where x is used here to include all the optimizations variables for each MPC.

3. Results and Discussions

3.1 Description of simulation case studies

3.1.1 Parameters of buildings

A prototype commercial building from a previous case study is used to generate the building clusters [54]. The sample building is a three stories commercial building. Building floor plans and constructions materials are known from design documents. Thermal resistance and capacitance are calculated based on the ASHRAE standard 90.1 [55]. Random factors drawn from a uniform distribution are further used to randomize the building parameters and sizes for a large-scale simulation. The internal load is determined by the ASHRAE standard definitions on the lighting and equipment power densities per meter square. Detailed building parameters are included in Appendix A.1. For the building HVAC system, one week of summer weather data collected by a local weather station at San Antonio are used as shown in Figure 6. The overall COPs of the HVAC systems in buildings are assumed to be constant and equal to 3. The maximum cooling power is limited to 330 KW per building. A night setback strategy for non-office hours is used for the HVAC baseline simulation. Office hours are defined from 7:30 am to 8:00 pm, while early start-up of the system is set from 7:00 am to 7:30 am. The set-point for office hours is 21.4°C ± 0.6 while the set-point for non-office hours is 23.5°C ± 0.5. After all parameters of the buildings are randomized, the physics models are obtained as detailed in Section 2.2.

All the commercial building occupancy profiles are simulated and generated using the LBNL occupancy simulator [41] to produce the synthetic occupancy data as the ground truth for individual buildings. The authors first introduce the occupancy density multiplier based on the randomized building size. Then, the original algorithm in [41] is modified to randomize the user-predefined parameters of the occupancy transitions among zones, including private cubicles, meeting spaces, auxiliary rooms, etc. The empirical rules based on the authors' previous occupancy studies [38] are used to define the upper and lower limits for the transition probabilities' randomizations. Lastly, the authors randomize the first arrival and the last departure times based on the previous occupancy study again [38]. For BtG MPC, each building occupancy profile generated by LBNL simulator is predicted in short term based on the algorithm presented in Section 2.1. The example occupancy profiles are presented using 965 randomized buildings in Figure 7.

3.1.2 Power Grid Parameters

Two standard IEEE power networks modeled in Matpower are used [51]: case 9 (9-bus system) and case 14 (14-bus system). For case 9, a total of 3 large generators are modeled to supply the power demand of 965 buildings while a total of 5 generators are modeled to supply 1058 buildings for case 14. The number of buildings for each case are decided based on the generation capacities and nominal bus loads predefined in Matpower. The parameters of the power network and the generator costs are all obtained from the provided casefiles in Matpower [51]. Examples of the grid parameters are listed in Appendix A.2. The real-time electricity prices for the same period as the weather data used are obtained from the Electric Reliability Council of Texas [56], as shown in Figure 8. The simulations are performed on MATLAB [57]. All occupancy, buildings, and grid are modeled and communicated through the authors' modularized Matlab functions, including the

interaction between the Matpower library and the LBNL simulator. All optimization problems are solved using CPLEX [58].

3.1.3 Simulation Cases

This study investigates three cases: 1) **DB&G**, 2) **BtG**, and 3) **OBtG**. For **DB&G**, the authors use the traditional bang-bang approach for building simulations and a grid MPC as shown in Eq. (21). The simulation entails that each building cluster has a corresponding processing unit that determines its own control law, while the grid is optimized and dispatched based on centralized optimization performed by the market operator (Figure 9 (a)). In **DB&G**, the building load is merely input to the grid. The building controls are assumed to use bang-bang control of ideal cooling demands. This means that the HVAC system only has two modes: "off" for no cooling, and "on" for ideal cooling to meet with loads. The cooling load is decided by

$$Q_{hvac} = C_{zone} m_{zone} (T_{zone} - T_{set}) \tag{23}$$

where Q_{hvac} is the cooling load, C_{zone} is the building thermal capacity, m_{zone} is the building thermal mass, T_{zone} is the building zone temperature, and T_{set} is the setpoint.

An alternative to the status-quo **DB&G**, a central **BtG** controller (as shown in Figure 9 (b)) collects all individual component (generators, buildings) parameters and constraints, including measurements, and solves the control problem with a global optimization function. The resulting optimization is a large-scale quadratic program as described in Section 2.4. Referring to Sections 2.4.1 to 2.4.2, **BtG** optimizes the buildings outputs of Eq. (18) as the inputs to Eq. (21) without any occupancy prediction. The night setback HVAC control strategy in **DB&G** is used again by embedding the assumed working schedules. An **OBtG** can be further proposed as the third simulation case for more energy savings and evaluations of the building thermal comforts. The

occupancy information such as presence and absence is predicted based on the innovative approach described in Section 2.1. The occupancy model simulates and predicts the occupancy state in terms of group behaviors at the whole building level. Two discomfort indexes are introduced to evaluate the potential violations of the comfort on people as

- Discomfort Index I (DI)

$$DI = \frac{\sum_{k=1}^{d} \left| T_{MPC}(k) - T_{set}(k) \right|}{d} \tag{24}$$

- Discomfort Index II (DII)

$$DII = \frac{\sum_{k=1}^{d} \Delta D}{d}$$
$$\text{s.t. } \Delta D = \begin{cases} T_{MPC} - T_{upper} & if \quad T_{MPC} > T_{upper} \\ T_{MPC} - T_{lower} & if \quad T_{lower} < T_{MPC} \\ 0 & else \end{cases} \tag{25}$$

where d is the length of the evaluated time horizon, T_{MPC} is the MPC optimized zone temperature, T_{set} is the setpoint temperature, T_{upper} and T_{lower} are the upper bound and lower bound of the zone temperatures respectively.

3.2 Results

3.2.1 Building thermal behavior

For **DB&G**, the HVAC is only operated when the simulated zone temperatures are outside the setpoint temperature bands. Consequently, **DB&G** turns the HVAC equipment on and off at a fast frequency to maintain the building temperatures around the setpoints, as shown in the top graph in Figure 10 (a). The office hour setpoints are 21.4°C while the non-office hour setbacks are 23.5°C. Building temperatures are maintained within the temperature bounds most of the time. Meanwhile,

the deviations of the zone temperatures for **DB&G** during night setback periods are smaller than the daytime periods of the office hours, as shown from the blue shades of the top graph in Figure 10 (a). Comparing the HVAC cooling powers of office hours and non-office hours of **DB&G** in Figure 10 (b), the cooling demands increase and decrease frequently during daytime (the large area of blue shades) due to the disturbance changes from the solar heat gain and outdoor air temperature. Thus, the zone temperatures frequently fluctuate and tend to deviate more from setpoints during office hours.

The performance of **BtG** is further depicted in Figure 10. For the first day of the simulation in Figure 10 (a), the zone temperatures of the building cluster evolve gradually up to the upper bounds (24.0°C) during non-office hours from the initial value (22.0°C), owing to the high setpoint of night setback periods. In the morning, overcooling occurs during the short start-up periods while the lower bounds of the office hours are reached. This is caused due to the high costs (50000$/Hz) on frequency deviations in the centralized BtG optimization of Eq. (25). Since the primary objective of power grid operators is to maintain stable operation, the frequency should always be as close as possible to 60 Hz to avoid damages to the grid's assets or in the worst case, black-outs. As a result, the $50,000/Hz cost is artificial in the sense but is preferred more than a $500/Hz cost, although a low cost (500$/HZ) on frequency deviations with same costs for other objectives gives no overcooling. After the overcooling, the zone temperatures return to the upper bound of office hours (22.0°C) very quickly. Near the end of the day, the evening setbacks gradually restore the zone temperatures to 24°C during the nights. The following days show similar temperature responses. However, zone temperatures are mostly maintained at 24°C for weekend periods except overcooling again in the morning. The results of cooling load from **BtG** as shown in Figure 10 (b),

comparing to **DB&G**, further illustrate the smoother load patterns and lower energy usages of the buildings.

The optimal start-up, lunch-break and setback time for **OBtG** are shown as the bottom graph in Figure 10 (a). Slightly higher zone temperature responses are observed at morning precooling (the blue line) period, noon break (the blue shade), and evening setbacks (the blue line) for each working day. It is worth noticing that the occupancy model predicts the absence periods if the aggregated occupancy presence shows that a majority of the people leave the offices. Hence, the constraints on the zone temperatures increase, thereby sacrificing the individual comfort of people who stay in the office during the optimized periods. The HVAC cooling load responses are further shown as the bottom graph in Figure 10 (b). Comparing to **BtG**, more consumption spikes are observed (the pink shade) due to the occupancy relaxations and their influences on the frequency responses of the grid operations are explored in the next section 3.2.2. Figure 11 further illustrates the difference between **BtG** and **OBtG** based on one day occupancy profile.

In **OBtG**, the uncertainty of the occupancy predictions may sacrifices occupants' comfort even when the majority of the people leave the office for lunch. Hence, the discomfort indexes of **DB&G**, **BtG**, and **OBtG** need to be analyzed and compared as shown in Table 1 for the simulated week. **DB&G** is robust enough with a deviation range around 0.11°C from the desired setpoint according to the comfort index DI. There are no violations beyond the upper and lower constraints during occupancy period, which is the same as **BtG**. Meanwhile, **BtG** allows more deviation (around 0.5°C) from the setpoint to save the energy consumption while maintaining the room temperatures in a comfort zone within the temperature constraints in Eq. (25). Compared to **BtG**, **OBtG** allows even more temperature deviation (up to 0.73°C) for the unoccupied period, although the uncertainty of the occupancy prediction creates difficulties to keep up with the constraints as

shown by DII index. However, the violation is small enough to be neglected and has no significant impact on the occupants' comfort.

3.2.2 Grid Performance

For **DB&G**, the coupling between the local and decoupled control actions of building clusters and the power system is achieved via the optimization of grid control inputs for the system-level performance objectives. The grid system control is using the same approach introduced in Section 2.4.2 for frequency regulation. In general, the grid MPC minimizes the electricity generation costs and maintains frequency stabilities during the grid operations. **DB&G** in Figure 12 (a) shows the example of IEEE Case 9 grid MPC based on the **DB&G** building controls. There are three types of grid load: the building base load, the building HVAC load, and the grid base load. Small spikes in Figure 12 (a) can be observed between the total generation and the total load for **DB&G** owing to the dynamic building HVAC load pattern. As the **DB&G** of Figure 10 (b) shows, the building HVAC load pattern exhibits large variations during the entire day, which causes the varied bus angles and frequency deviation depicted in Figures 12 (b) and (c). In conclusion, **DB&G** can handle certain level of dynamic changes of the load pattern, as shown by the small spikes of all the bus angles in Figure 12 (b) and frequency deviations in Figure 12 (c) during some periods.

However, it is obvious that **BtG** is necessary since very large spikes of the frequencies are observed for **DB&G** of Figure 12 (c) at certain periods. Smoother responses from the bus angles of **BtG**, shown in Figure 12 (b), are detected by comparing to **DB&G**. **BtG** also has fewer mismatch spikes between the total grid generation and the total grid load in Figure 12 (a). In Figure 12 (c), a significant reduction in frequency deviations can be found when comparing **DB&G** with **BtG**. The frequency during all simulation periods is also very close to nominal value (60 Hz) for **BtG**.

Overall, **BtG** shows a more stable and cost effective optimization on both building and grid systems.

Last but not least, **OBtG** has little cost impacts on the grid operations, as shown from **OBtG** plots in Figure 12. In Figure 12(a), the total grid load is consistently balanced by the total grid generation except the morning periods for **OBtG**. The mismatch spikes in the morning is caused by the occupancy-based rescheduling of the cooling start time. A more dynamic pattern of the cooling load can be observed at the precooling stages as shown from **OBtG** in Figure 10 (b). Compared with **BtG**, the bus angles and frequency responses are very similar and stable. In general, no significant impacts from **OBtG** can be observed on the grid operations although **OBtG** alters the HVAC load patterns of the individual buildings.

3.3 Extended simulations and results

Extended simulations are performed on the IEEE Case 14 grid system with similar testing configurations as explained in Sections 2.1 through 2.4. This section provides the detailed cost analysis in Table 2 based on simulations of Case 9 and Case 14 for all tested scenarios: **DB&G**, **BtG**, and **OBtG**. Comparing frequency penalties for the three scenarios, there are significant decreases of the frequency costs during the grid operations when **BtG** and **OBtG** are used. As discussed before, the grid frequencies experience very high deviations from the nominal value (60 Hz) for the Case 9 **DB&G** simulation, as shown in Figure 12 (c). However, the frequency deviations for **BtG** and **OBtG** are less noticeable. Similar observations can be made for the Case 14 simulation. In contrast, the costs for electricity generations from the generators are very close to each other for all test scenarios. Maximum 2% of cost saving can be observed for both Case 9 and Case 14 systems, although the maximum absolute saving amount is around 34 thousand dollars. Meanwhile, the building costs based on the real time price show higher savings for **OBtG**

and **BtG** comparing to **DB&G**. The maximum saving is around 5.4% for **BtG** and around 6.7 % for **OBtG** during a whole week simulation. The largest saving amount is around 276 thousand dollars. By calculating the total costs, it is clear that **BtG** already has very large saving potential while **OBtG** slightly improves the system performance. The total savings for **BtG** and **OBtG** of Case 9 comparing to baseline are 60% and 61% respectively. The total savings for **BtG** and **OBtG** of Case 14 comparing to baseline are 50% and 51% respectively.

4. Conclusions

This paper develops and demonstrates new algorithms that facilitate the interaction of building load controls with power grid, leading to an occupancy-based Buildings-to-Grid integration. The study introduces a simulation framework that explicitly includes all detailed physics models of the occupancy, the buildings, and the grid at community scale for high-level optimization. Occupancy-based air conditioning model predictive control for building clusters is developed for reducing billing costs and maintaining comfort satisfaction. Additionally, optimal power flow problems for frequency control are explored for two standard power systems. The simulations are performed using real data collected from a local weather station, ground truth prices, and occupancy information to mimic the practical cases. Simulations show significant reduction of frequency deviations for grid operations (99%) while fair cost savings for electricity generations (1-2%) and building billings (5-7%). This centralized framework can be used for day-ahead planning to reduce the real-time grid control and communication problems for smart cities. A grid system operator ideally could solve the BtG integration problem proposed in this study to let the commercial building managers to response to the globally optimized routine. The framework is useful for city scale planning and operation evaluations for energy industry and utility operators.

The larger contribution of operation cost saving on frequency regulation is similar to some studies' findings that use BtG integration at smaller scale in terms of the number of buildings [7-8]. More ancillary services could be provided by buildings [6,9,11,15-16], but building occupancy comforts and operation costs are rarely considered jointly [10]. This study demonstrate the potential to design and optimize an integrated **BtG** platform with detailed physics models for occupancy, buildings, and grids. However, the performance of **OBtG** with occupancy forecasts is similar to **BtG** because of the night setback strategy. The night setback is already indicating an occupancy-based scheduling since the main vacancy period of office occupancy is the night time. Thus, **OBtG** could only improve energy efficiency for buildings up to a reasonable level (up to 2% difference) by optimizing other shorter absence periods (e.g. lunch breaks). On the other hand, occupancy information of Type II, number of people in a building, could be more valuable for controlling building operations. For example, the ventilation air flow depends on the number of people. By integrating with more occupancy information and control objectives, more savings on the grid generation and building billings could be expected, which will be an extension of this study.

It is also noticed that the centralized BtG MPC uses a simplified building thermal network model for a large-scale optimization problem in this study. The benefit is to provide a feasible optimal solution for fast decision-making of a utility operator. It is possible to extend the current study to include complex building and grid models, namely high-order thermal networks such as Energyplus and power grid models, to achieve multi-objective optimization in the BtG integration. For example, the optimization problem could be joint regulation of the grid voltage and frequency [59-61], optimization of the building demand response [62-63], etc. However, this will yield a much more complex optimization problem and computation cost. The foreseen optimization problem would no longer be a simple quadratic program. Other limitations of the study are brought

by the centralized optimization design. The centralized structure is not practical for systems with a very large number of buildings at a city scale, while privacy concerns from building operators also likely not allow collecting all relevant building parameters and control constraints to the system operator. To alleviate these issues, distributed approaches could be alternatively explored but are beyond the scope of the present study.

5 Acknowledgement

This research is supported by the National science foundation (NSF) titled: Collaborative Research: Empowering Smart Energy Communities: Connecting Buildings, People, and Power Grids, Award Number: 1637249**.**

6 References

1. Hagerman, J., 2013. Buildings to Grid Integration & Interoperability. Technical Lecture. Office of Energy Efficiency and Renewable Energy and Building Technologies office. U.S. Department of Energy.
2. Hagerman, J., 2015. EERE & Buildings to Grid Integrations. Office of Energy Efficiency and Renewable Energy and Building Technologies office. U.S. Department of Energy.
3. Buildings-to-Grid Integration. U.S. Department of Energy. Accessed at: https://energy.gov/eere/buildings/buildings-grid-integration.
4. Labeodan, T., Aduda, K., Boxem, G. and Zeiler, W., 2015. On the application of multi-agent systems in buildings for improved building operations, performance and smart grid interaction–A survey. *Renewable and Sustainable Energy Reviews*, *50*, pp.1405-1414.
5. Qi, J., Kim Y.J., Chen. C., Lu, X., and Wang, J., 2016. Demand response and smart buildings: A survey of control, communication, and cyber-physical security. *ACM Trans. Cyber-Physical Systems*, *1*(3), pp. 1-28.
6. Razmara, M., Bharati, G.R., Shahbakhti, M., Paudyal, S. and Robinett III, R.D., 2016. Bilevel Optimization Framework for Smart Building-to-Grid Systems. *IEEE Transactions on Smart Grid*, *99*, pp.1-1.
7. Maasoumy, M., Sanandaji, B.M., Sangiovanni-Vincentelli, A. and Poolla, K., 2014. Model predictive control of regulation services from commercial buildings to the smart grid. In *American Control Conference (ACC), 2014* (pp. 2226-2233). IEEE.
8. Zhao, P., Henze, G.P., Brandemuehl, M.J., Cushing, V.J. and Plamp, S., 2015. Dynamic frequency regulation resources of commercial buildings through combined building system resources using a supervisory control methodology. *Energy and Buildings*, *86*, pp.137-150.

9. Xue, X., Wang, S., Yan, C. and Cui, B., 2015. A fast chiller power demand response control strategy for buildings connected to smart grid. Applied Energy, 137, pp.77-87.
10. Lin, Y., Barooah, P. and Mathieu, J.L., 2017. Ancillary services through demand scheduling and control of commercial buildings. *IEEE Transactions on Power Systems*, *32*(1), pp.186-197.
11. Zhao, Y., Lu, Y., Yan, C. and Wang, S., 2015. MPC-based optimal scheduling of grid-connected low energy buildings with thermal energy storages. *Energy and Buildings*, *86*, pp.415-426.
12. Lu, Y., Wang, S. and Shan, K., 2015. Design optimization and optimal control of grid-connected and standalone nearly/net zero energy buildings. *Applied Energy*, *155*, pp.463-477.
13. Costanzo, G.T., Zhu, G., Anjos, M.F. and Savard, G., 2012. A system architecture for autonomous demand side load management in smart buildings. *IEEE Transactions on Smart Grid*, *3*(4), pp.2157-2165.
14. Di Giorgio, A. and Liberati, F., 2014. Near real time load shifting control for residential electricity prosumers under designed and market indexed pricing models. Applied Energy, 128, pp.119-132.
15. Shao, S., Pipattanasomporn, M. and Rahman, S., 2012. Grid integration of electric vehicles and demand response with customer choice. *IEEE transactions on smart grid*, *3*(1), pp.543-550.
16. Xue, X., Wang, S., Sun, Y. and Xiao, F., 2014. An interactive building power demand management strategy for facilitating smart grid optimization. *Applied Energy*, *116*, pp.297-310.
17. Lawrence, T.M., Boudreau, M.C., Helsen, L., Henze, G., Mohammadpour, J., Noonan, D., Patteeuw, D., Pless, S. and Watson, R.T., 2016. Ten questions concerning integrating smart buildings into the smart grid. *Building and Environment*, *108*, pp.273-283.
18. Klepeis, N.E., Nelson, W.C., Ott, W.R., Robinson, J.P., Tsang, A.M., Switzer, P., Behar, J.V., Hern, S.C. and Engelmann, W.H., 2001. The National Human Activity Pattern Survey (NHAPS): a resource for assessing exposure to environmental pollutants. *Journal of Exposure Science and Environmental Epidemiology*, *11*(3), p.231.
19. National Grid. 2002. Managing Energy Costs in Office Buildings. Available at: https://www9.nationalgridus.com/non_html/shared_energyeff_office.pdf.
20. Oldewurtel, F., Sturzenegger, D. and Morari, M., 2013. Importance of occupancy information for building climate control. *Applied energy*, *101*, pp.521-532.
21. Goyal, S., Ingley, H.A. and Barooah, P., 2013. Occupancy-based zone-climate control for energy-efficient buildings: Complexity vs. performance. *Applied Energy*, *106*, pp.209-221.
22. Xu, P., Haves, P., Piette, M.A. and Braun, J., 2004. Peak demand reduction from pre-cooling with zone temperature reset in an office building. *Lawrence Berkeley National Laboratory*.
23. Oldewurtel, F., Sturzenegger, D. and Morari, M., 2013. Importance of occupancy information for building climate control. Applied energy, 101, pp.521-532.

24. Mirakhorli, A. and Dong, B., 2016. Occupancy behavior based model predictive control for building indoor climate—A critical review. *Energy and Buildings*, *129*, pp.499-513.
25. Široký, J., Oldewurtel, F., Cigler, J. and Prívara, S., 2011. Experimental analysis of model predictive control for an energy efficient building heating system. Applied energy, 88(9), pp.3079-3087.
26. Chen, X., Wang, Q. and Srebric, J., 2016. Occupant feedback based model predictive control for thermal comfort and energy optimization: A chamber experimental evaluation. Applied energy, 164, pp.341-351.
27. Dong, B. and Lam, K.P., 2014, February. A real-time model predictive control for building heating and cooling systems based on the occupancy behavior pattern detection and local weather forecasting. In *Building Simulation* (Vol. 7, No. 1, pp. 89-106). Springer Berlin Heidelberg.
28. Erickson, V.L., Carreira-Perpiñán, M.Á. and Cerpa, A.E., 2014. Occupancy modeling and prediction for building energy management. *ACM Transactions on Sensor Networks (TOSN)*, *10*(3), p.42.
29. Dobbs, J.R. and Hencey, B.M., 2014. Model predictive HVAC control with online occupancy model. *Energy and Buildings*, *82*, pp.675-684.
30. Wang, D., Federspiel, C.C. and Rubinstein, F., 2005. Modeling occupancy in single person offices. *Energy and buildings*, *37*(2), pp.121-126.
31. Chen, Z. and Soh, Y.C., 2016. Comparing occupancy models and data mining approaches for regular occupancy prediction in commercial buildings. *Journal of Building Performance Simulation*, pp.1-9.
32. D'Oca, S. and Hong, T., 2015. Occupancy schedules learning process through a data mining framework. *Energy and Buildings*, *88*, pp.395-408.
33. Andrews, C.J., Yi, D., Krogmann, U., Senick, J.A. and Wener, R.E., 2011. Designing buildings for real occupants: An agent-based approach. *IEEE Transactions on Systems, Man, and Cybernetics-Part A: Systems and Humans*, *41*(6), pp.1077-1091.
34. Shaikh, P.H., Nor, N.B.M., Nallagownden, P., Elamvazuthi, I. and Ibrahim, T., 2014. A review on optimized control systems for building energy and comfort management of smart sustainable buildings. *Renewable and Sustainable Energy Reviews*, *34*, pp.409-429.
35. Tuballa, M.L. and Abundo, M.L., 2016. A review of the development of Smart Grid technologies. *Renewable and Sustainable Energy Reviews*, *59*, pp.710-725.
36. Camarinha-Matos, L.M., 2016. Collaborative smart grid–A survey on trends. *Renewable and Sustainable Energy Reviews*, *65*, pp.283-294.
37. Yan, D., O'Brien, W., Hong, T., Feng, X., Gunay, H.B., Tahmasebi, F. and Mahdavi, A., 2015. Occupant behavior modeling for building performance simulation: Current state and future challenges. *Energy and Buildings*, *107*, pp.264-278.
38. Li, Z. and Dong, B., 2017. A new modeling approach for short-term prediction of occupancy in residential buildings. *Building and Environment*, *121*, pp.277-290.
39. Erickson, V.L. and Cerpa, O.., 2010. Occupancy-Based System for Efficient Reduction of HVAC Energy. In *Proc. of the 10th International Conference on Information Processing in Sensor Networks (IPSN'11)*.
40. Liu, S., Yamada, M., Collier, N. and Sugiyama, M., 2013. Change-point detection in time-series data by relative density-ratio estimation. *Neural Networks*, *43*, pp.72-83.

41. Chen, Y., Hong, T. and Luo, X., 2018, February. An agent-based stochastic Occupancy Simulator. In Building Simulation (Vol. 11, No. 1, pp. 37-49). Tsinghua University Press.
42. Patel, N.R., Rawlings, J.B., Wenzel, M.J. and Turney, R.D., 2016. Design and Application of Distributed Economic Model Predictive Control for Large-Scale Building Temperature Regulation. In *Purdue International High Performance Buildings Conferenc*e, *2016*.
43. Patel, N.R., Risbeck, M.J., Rawlings, J.B., Wenzel, M.J. and Turney, R.D., 2016, July. Distributed economic model predictive control for large-scale building temperature regulation. In *American Control Conference (ACC), 2016* (pp. 895-900). IEEE.
44. Putta, V.K., Kim, D., Cai, J., Hu, J. and Braun, J.E., 2014. Distributed model predictive control for building HVAC systems: a case study. *In Purdue International High Performance Buildings Conference, 2014*.
45. Park, H., Ruellan, M., Bouvet, A., Monmasson, E. and Bennacer, R., 2011, October. Thermal parameter identification of simplified building model with electric appliance. In *Electrical Power Quality and Utilisation (EPQU), 2011 11th International Conference on* (pp. 1-6). IEEE.
46. Braun, J.E. and Chaturvedi, N., 2002. An inverse gray-box model for transient building load prediction. *HVAC&R Research*, *8*(1), pp.73-99.
47. Zhou, Q., Wang, S., Xu, X. and Xiao, F., 2008. A grey-box model of next-day building thermal load prediction for energy-efficient control. *International Journal of Energy Research*, *32*(15), pp.1418-1431.
48. Dong, B., Gorbounov, M., Yuan, S., Wu, T., Srivastav, A., Bailey, T. and O'Neill, Z., 2013, September. Integrated energy performance modeling for a retail store building. In *Building Simulation* (Vol. 6, No. 3, pp. 283-295). Tsinghua University Press.
49. O'Neill, Z., Narayanan, S. and Brahme, R., 2010. Model-based thermal load estimation in buildings. *IBPSA-USA Journal*, *4*(1), pp.474-481.
50. Taha, A.F., Gatsis, N., Dong, B., Pipri, A. and Li, Z., 2017. Buildings-to-Grid Integration Framework. IEEE Transactions on Smart Grid.
51. Zimmerman, R.D., Murillo-Sánchez, C.E. and Thomas, R.J., 2011. MATPOWER: Steady-state operations, planning, and analysis tools for power systems research and education. *IEEE Transactions on power systems*, *26*(1), pp.12-19.
52. Low, S.H., 2014. Convex relaxation of optimal power flow—Part I: Formulations and equivalence. *IEEE Transactions on Control of Network Systems*, *1*(1), pp.15-27.
53. Giannakis, G.B., Kekatos, V., Gatsis, N., Kim, S.J., Zhu, H. and Wollenberg, B.F., 2013. Monitoring and optimization for power grid: A signal processing perspective. *IEEE Signal Processing Magazine*, *30*(5), pp.107-128.
54. Li, Z. and Vega, R., 2015. A Hybrid Model for Electrical Load Forecasting-a New Approach Integrating Data-Mining with Physics-Based Models. *ASHRAE Transactions*, *121*.
55. Thornton, B.A., Rosenberg, M.I., Richman, E.E., Wang, W., Xie, Y., Zhang, J., Cho, H., Mendon, V.V., Athalye, R.A. and Liu, B., 2011. *Achieving the 30% goal: Energy and cost savings analysis of ASHRAE Standard 90.1-2010* (No. PNNL-20405). Pacific Northwest National Laboratory (PNNL), Richland, WA (US).
56. Electric Reliability Council of Texas. 2016. Accessed at: http://www.ercot.com/mktinfo/prices.

57. Matlab R2016b. 2016. Matworks. Inc.
58. CPLEX, I.I., 2009. V12. 1: User's Manual for CPLEX. *International Business Machines Corporation*, *46*(53), p.157.
59. Garces, A., 2016. A linear three-phase load flow for power distribution systems. IEEE Transactions on Power Systems, 31(1), pp.827-828.
60. Kekatos, V., Zhang, L., Giannakis, G.B. and Baldick, R., 2016. Voltage regulation algorithms for multiphase power distribution grids. IEEE Transactions on Power Systems, 31(5), pp.3913-3923.
61. Li, Z., Guo, Q., Sun, H. and Wang, J., 2016. Coordinated economic dispatch of coupled transmission and distribution systems using heterogeneous decomposition. IEEE Transactions on Power Systems, 31(6), pp.4817-4830.
62. Broeer, T., Fuller, J., Tuffner, F., Chassin, D. and Djilali, N., 2014. Modeling framework and validation of a smart grid and demand response system for wind power integration. Applied Energy, 113, pp.199-207.
63. Wang, Q., Zhang, C., Ding, Y., Xydis, G., Wang, J. and Østergaard, J., 2015. Review of real-time electricity markets for integrating distributed energy resources and demand response. Applied Energy, 138, pp.695-706.

Appendix A:

A.1: Building system parameters.

Recalling from Section 2.2, the example Case 9 BtG randomization in this study produces the building parameters as follows:

	$R_1(^\circ C/W)$	$R_2(^\circ C/W)$	$R_{win}(^\circ C/W)$	$C_{zone}(1/^\circ C)$	$C(1/^\circ C)$
min	2.57×10^{-5}	2.57×10^{-5}	0.85×10^{-2}	4.53×10^{7}	1.15×10^{9}
mean	5.80×10^{-5}	5.81×10^{-5}	1.68×10^{-2}	9.72×10^{7}	2.34×10^{9}
max	1.21×10^{-4}	1.22×10^{-4}	2.54×10^{-2}	1.89×10^{8}	4.86×10^{9}

A.2: Grid system parameters.

The grid system parameters are extracted from the Matpower6.0 b1 version. Recalling from Section 2.3, the example of 210 MVA Case 9 BtG in this study uses the IEEE 9 bus system parameters:

1) Buses loads:

Bus Number	**1**	**2**	**3**	**4**	**5**	**6**	**7**	**8**	**9**
Limit (MW)	0	0	0	0	189	0	210	0	262

2) Branch transmission:

Branch	**1-4***	**4-5**	**5-6**	**3-6**	**6-7**	**7-8**	**8-2**	**8-9**	**9-4**
Susceptance	17.36	10.86	5.88	17.06	9.92	13.88	16	6.21	11.76

***The brunch 1-4 means the branch from bus No.1 to No. 4.

3) Generator cost:

Generator	Quadratic($/MW^{2}h)	Linear ($/MWh)	Constant ($)
1	0.11	5	150
2	0.085	1.2	600
3	0.1225	1	335

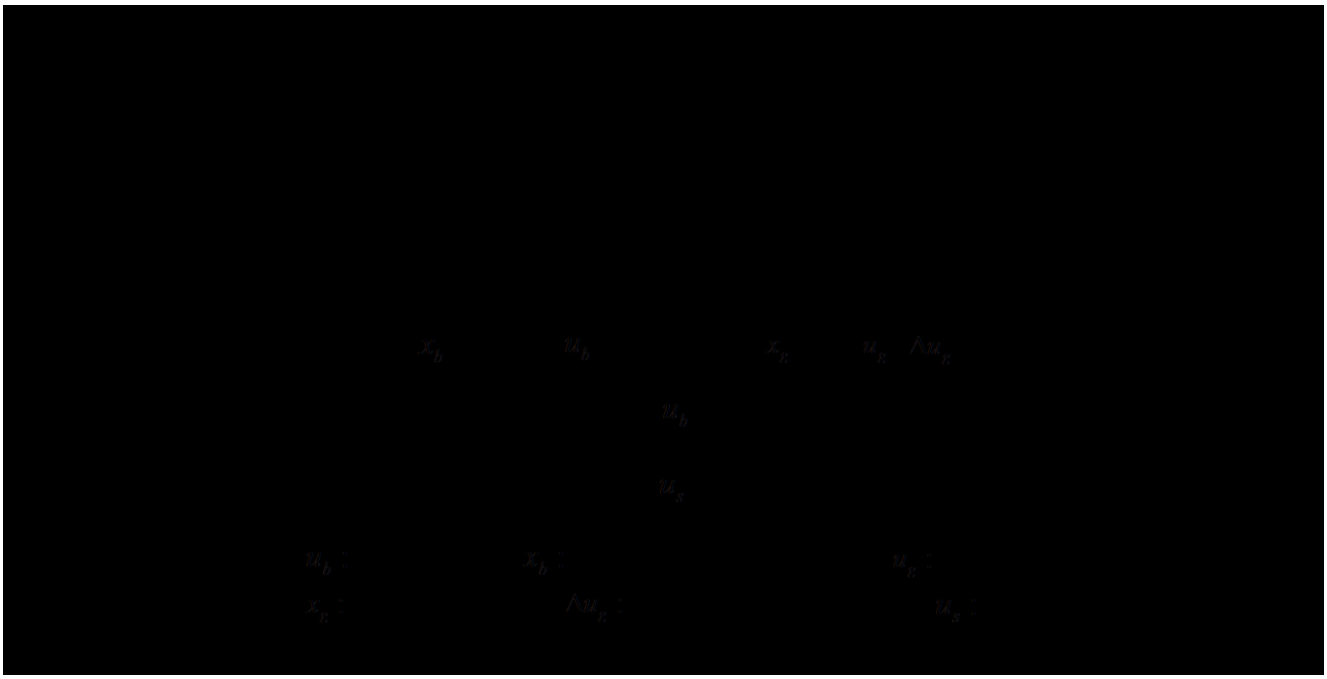

Figure 1. Schematics for the BtG MPC framework.

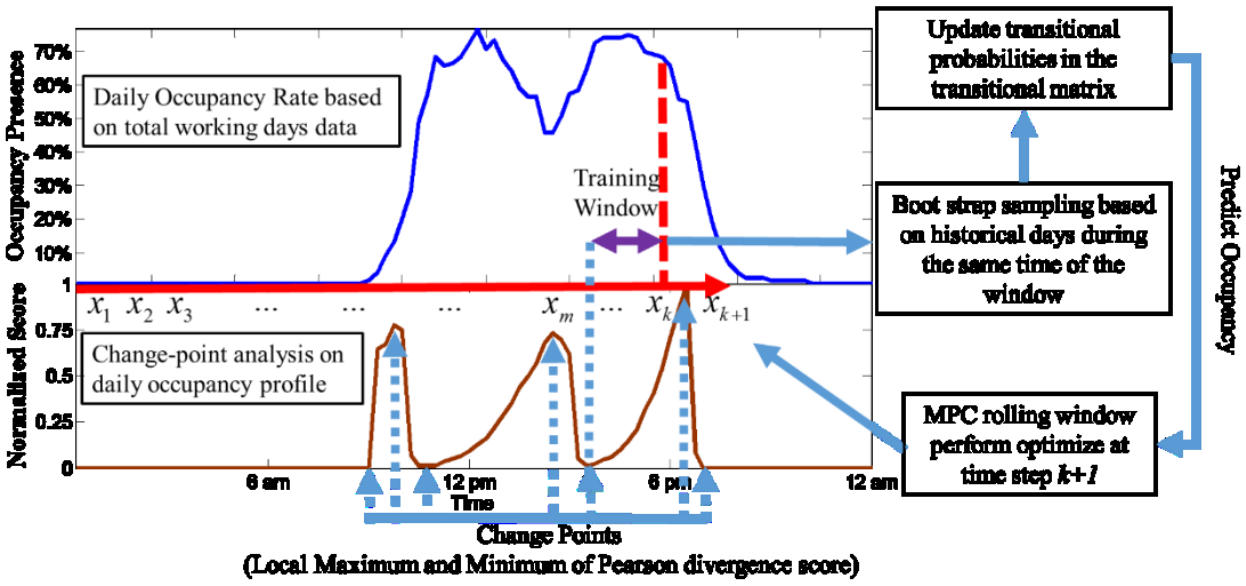

Figure 2. Occupancy model training and predicting in a rolling MPC [38].

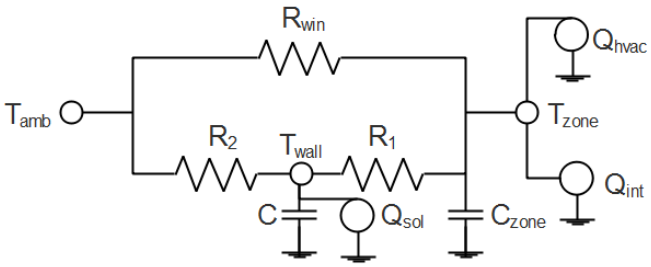

Figure 3. 2R-1C Thermal Network [50].

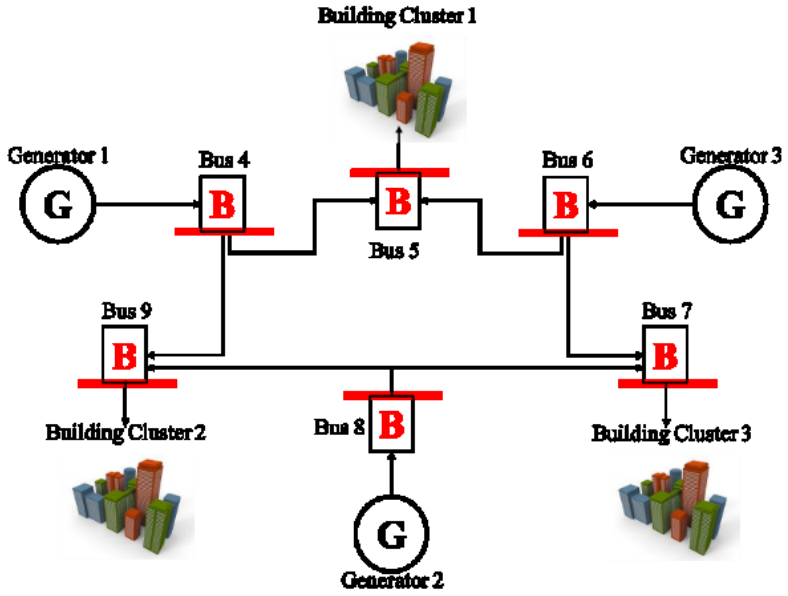

Figure 4. A hypothetical grid system.

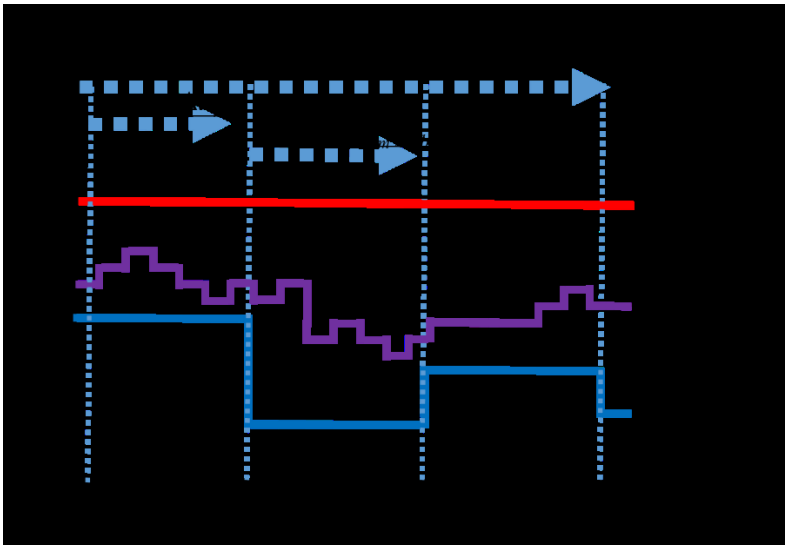

Figure 5. BtG MPC at three levels of time periods.

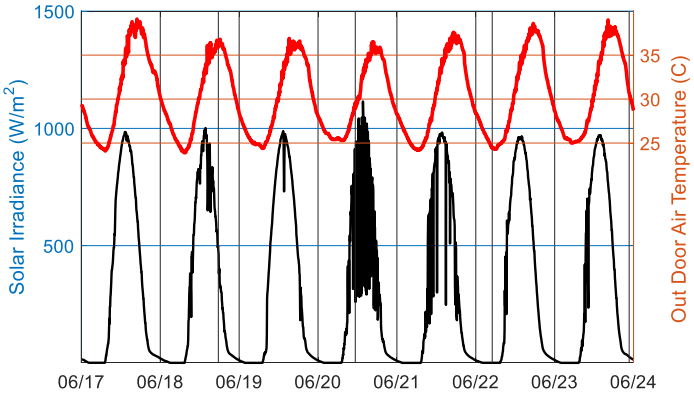

Figure 6. The outdoor air temperature and the horizontal solar irradiance.

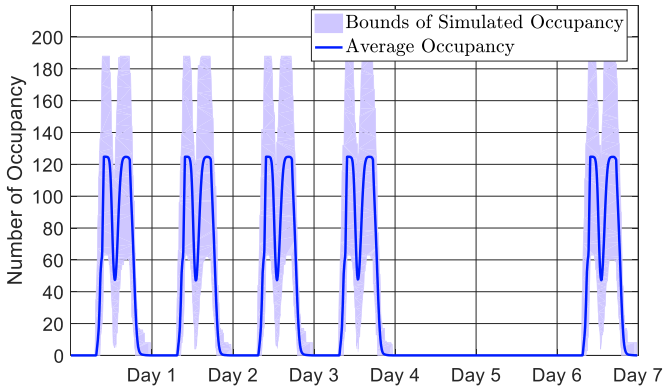

Figure 7. The occupancy profiles from the modified LBNL simulator for large-scale building cluster simulations.

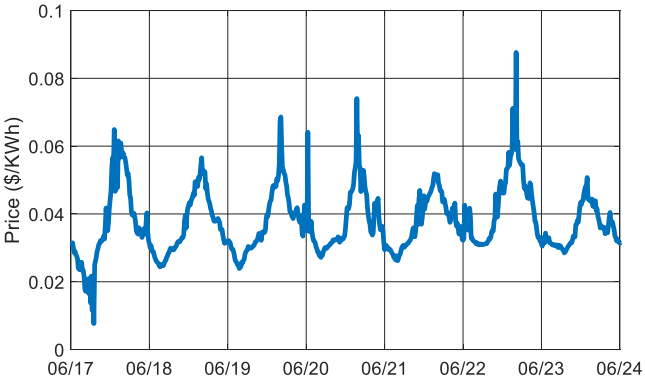

Figure 8. Electricity prices from Electric Reliability Council of Texas [56].

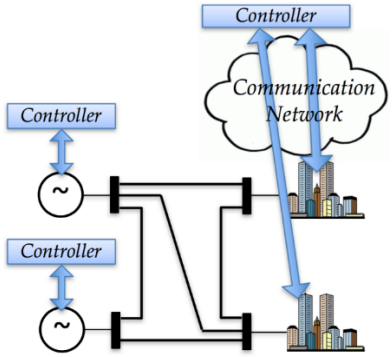

(a) A decoupled control

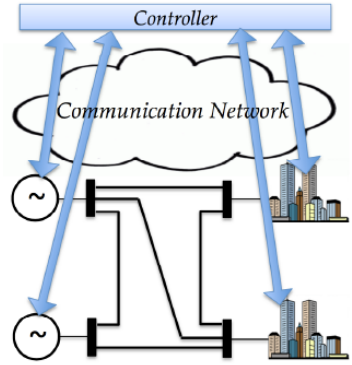

(b) A centralized control

Figure 9. Different control scenarios.

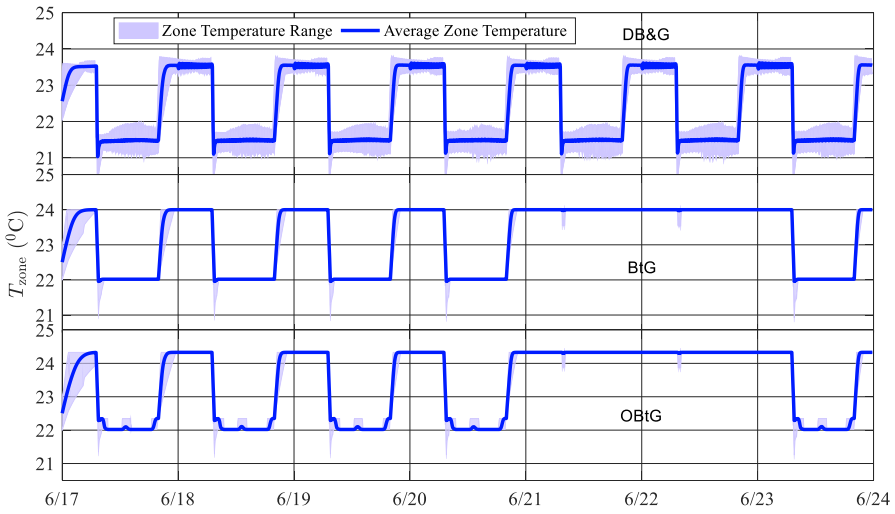

(a) Zone temperature responses

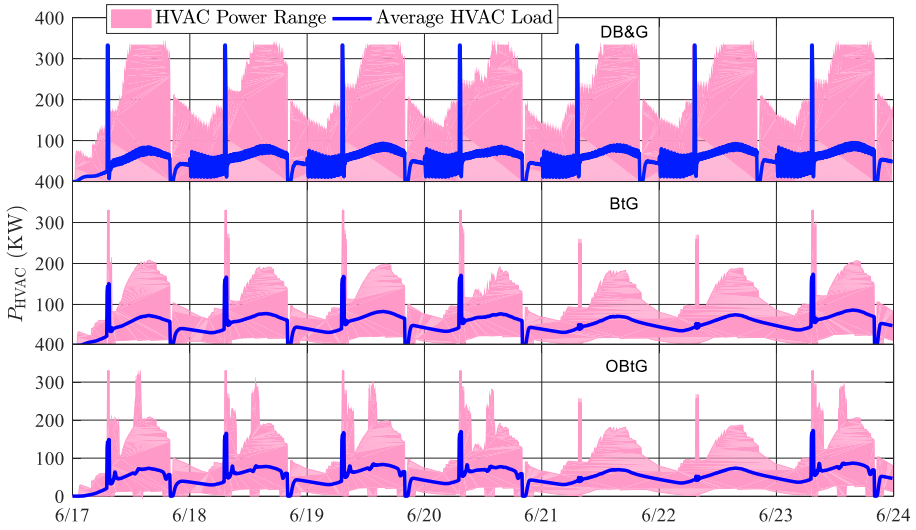

(b) Building cooling power

Figure 10. Performance of building within the BtG framework.

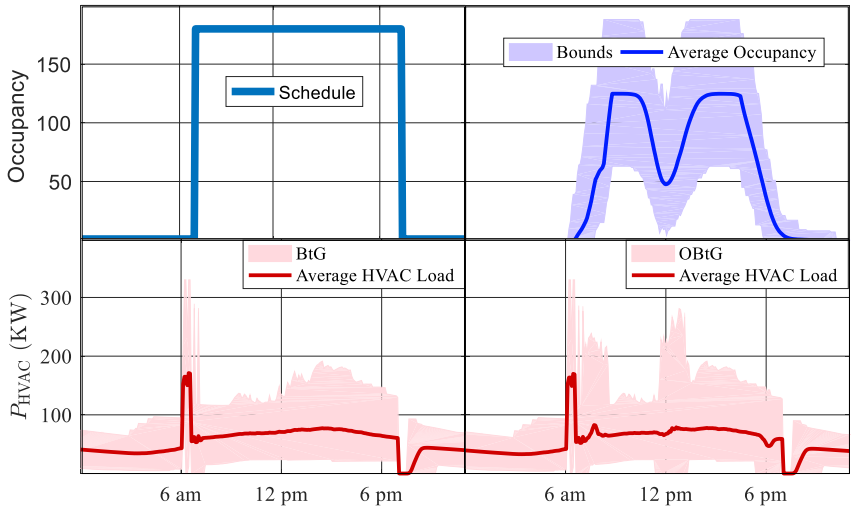

Figure 11. One-day comparison between the BtG MPC and the occupancy-based BtG MPC

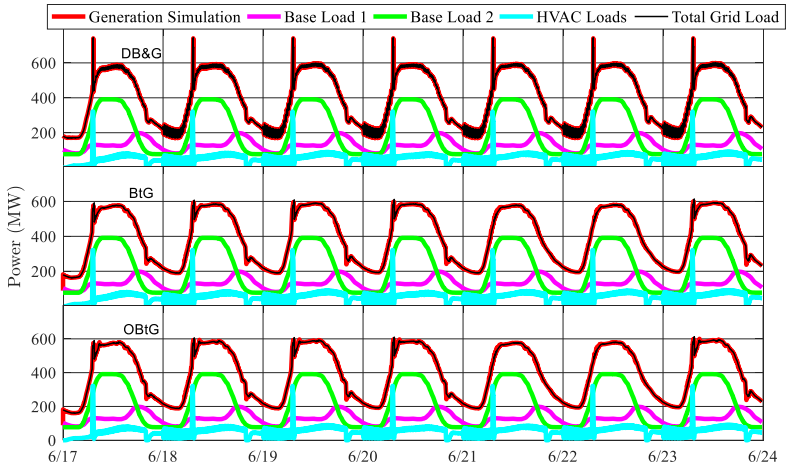

(a) Total grid generation and other loads (Base Load 1: The grid' base load; Base Load 2: The buildings' bases load; HVAC Load: The buildings' cooling load).

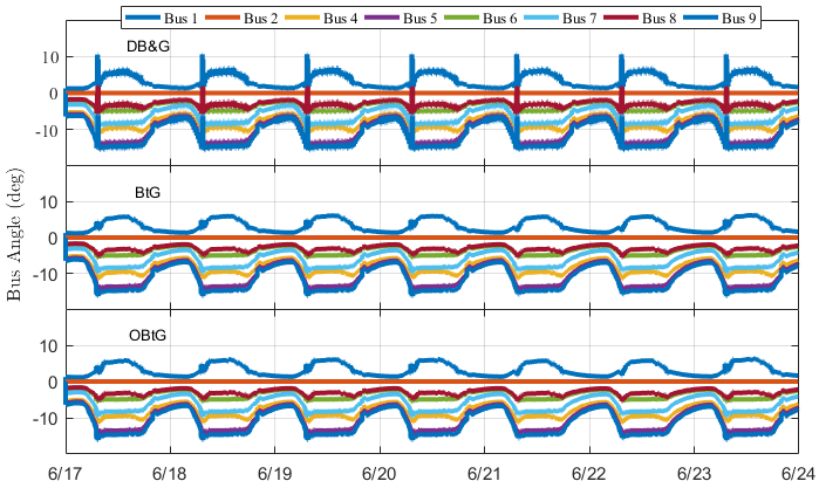

(b) Grid buses' angle changes with Bus 3 as the reference bus.

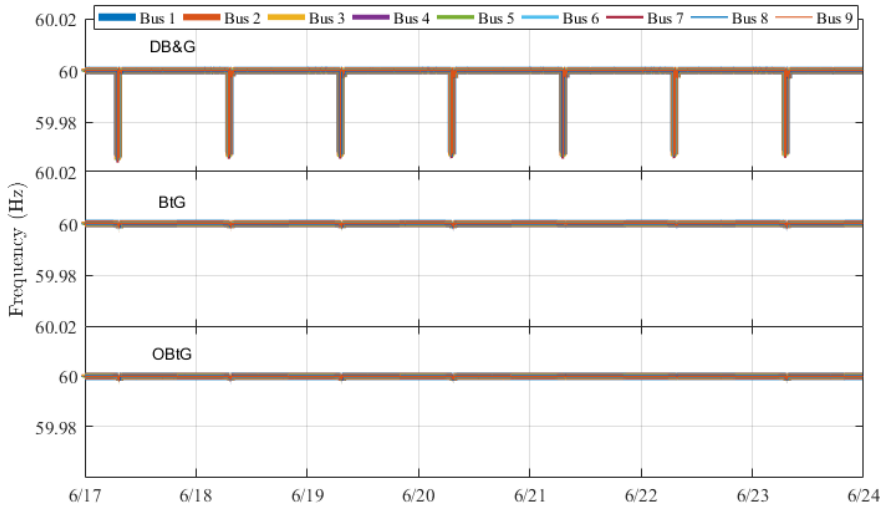

(c) Grid frequency responses

Figure 12. Performance of building within the BtG framework

Table 1 Discomfort Indexes per day for Case 9

	DB&G		**BtG**		**OBtG**	
	DI*	DII*	DI	DII	DI	DII
06/17	0.1102	0	0.5043	0	0.7310	0.0044
06/18	0.1086	0	0.50358	0	0.7312	0.0045
06/19	0.1157	0	0.5043	0	0.7303	0.0046
06/20	0.1102	0	0.5042	0	0.7305	0.0046
06/23	0.1191	0	0.5044	0	0.7299	0.0045

*All units for DI and DII presented are in °C.

Table 2 Cost comparison for all scenarios (unit of cost in 1000$).

Test Case	Cost Type	**DB&G**	**BtG**	**OBtG**
Case 9	Frequency Penalty	7493.09	6.63 (99%)	6.64 (99%)
	Generator Generation	1650.61	1618.43 (1.9%)	1616.45 (2.1%)
	Building Energy Cost	3647.29	3462.91 (5.1%)	3415.11 (6.8%)
	Total BtG Cost	**12790.99**	**5087.98 (60%)**	**5038.21 (61%)**
Case 14	Frequency Penalty	6396.10	5.95 (99%)	11.58 (99%)
	Generator Generation	2673.56	2659.06 (0.5%)	2651.17 (0.8%)
	Building Energy Cost	4065.12	3845.87 (5.4%)	3789.68 (6.7%)
	Total BtG Cost	**13134.79**	**6510.89 (50%)**	**6452.44(51%)**